Generation of Stems in Streamer Corona of Negative Leader

Dmitry Iudin[1, 2, 3,*], Artem Syssoev[1, 2], Nikolay Popov[4]

1. Institute of Applied Physics of the Russian Academy of Sciences, Nizhny Novgorod, Russia
2. Space Research Institute of Russian Academy of Science, Moscow, Russia
3. Federal State Budgetary Educational Institution of Higher Education "Nizhny Novgorod State University of Architecture and Civil Engineering", Nizhny Novgorod, Russia
4. Skobel'tsyn Institute of Nuclear Physics, Moscow State University, Moscow, Russia

ABSTRACT: It's known that overwhelming majority (up to 90%) of cloud-to-ground lightning discharges is provided by negative leaders, which, in contradistinction to positive ones, develop in stepped manner. Each new step appears when a positive part of bipolar space leader, growing from a space stem, contacts with the primary negative leader tip. It's believed that space stems, which are small polarized plasma formations of the volume of about 1 cm3 elongated along the local electric field direction, form ahead of negative leader head during negative corona streamer burst, the final stage of the step formation process accompanied by intensive negative charge eruption. Despite the stepped leaders have been discovered more than 100 years ago, it's still unknown what ensures the stepped mechanism of a negative leader development. The picture of stems genesis ahead of the negative leader remains still enigmatic. There is no any plausible hypothesis or numerical model explaining stem formation process in conditions when an ambient electric field magnitude inside a negative leader corona is several times less than the dielectric strength of air. In this study we propose a new scenario, where generation of stems in streamer corona of negative leader is considered as a noise-induced nonequilibrium phase transition. The main mechanism is based on the ionization process occurring at the external boundary of the negative leader corona in the presence of strongly inhomogeneous stochastic electric field relief. The last is formed by chaotically positioned clusters of negative charge transported to the negative streamer zone volume by negative streamer heads during negative streamer corona bursts. We took into account the fact that electron detachment from negative ions can also have impact on the ionization rate, especially at elevated electric fields. A cellular automaton model is established that reproduces the stem formation times at different altitudes above sea level.

INTRODUCTION

It's known that overwhelming majority (up to 90% [*Rakov and Uman*, 2003]) of cloud-to-ground lightning discharges is provided by negative leaders, which, in contradistinction

* Contact information: Dmitry Iudin, Institution, Institute of Applied Physics of the Russian Academy of Sciences, Nizhny Novgorod, Russia, Email: iudin@ipfran.ru

to positive ones, develop in stepped manner [*Rakov and Uman*, 2003; *Bazelyan and Raizer*, 2000]. Each new step appears when a positive part of bipolar space leader, growing from space stem, contacts with the primary negative leader tip. This results in almost instantaneous jump of negative leader tip, bearing high negative leader channel potential, to the point of bipolar space leader negative end, warming-up a new channel segment, and powerful negative corona streamer burst from newly-formed negative leader tip. It's believed that space stems, which are small plasma formations with a volume of about 1 cm^3 elongated along the local electric field direction, are formed ahead of the negative leader head during negative corona streamer burst, thereby closing the step formation cycle. More information about the negative stepped leader development process can be found, for example, in [*Rakov and Uman*, 2003].

Despite the stepped leaders have been discovered more than 100 years ago (see, for example, *Uman* [1969] and references therein), it's still unknown what ensures the stepped mechanism of a negative leader development. *Bazelyan and Raizer* [2000] characterize the picture of space stem genesis ahead of the negative leader head as "nearly mystic". As far as we know, there is no any plausible hypothesis or numerical model explaining physics of space stem formation process. In some way this conundrum is close to the problem of lightning initiation, because in both cases one needs the presence of ionization centers to release streamer breakdown, which consequently turns into the leader form. There are two main hypotheses concerning the lightning leader formation process (see *Petersen et al.* [2008] and references therein). The first was proposed by *Gurevich et al.* [1992] and is based on the runaway breakdown process. The second one, originated in the work of *Loeb* [1966], is associated with the positive streamers initiating from a hydrometeor (see, for example, [*Babich et al*, 2016; *Dubinova et al*, 2015; *Sadighi et al.*, 2015]) or a pair of approaching hydrometeors (see, for example, [*Cai et al*, 2017]) and works only under the preliminary ionization condition. In the resent work of *Iudin* [2017] there was proposed a fundamentally new mechanism of lightning initiation based on noise-induced phase transition supported by electrons detachment from negative ions, where the spatial noise is provided with sparking originating from charged hydrometeors interaction. Detailed overview of presently existing lightning initiation scenarios can be found in the work of *Iudin* [2017].

The peculiarity of the space leader formation process is that there are no any hydrometeors in the negative leader streamer zone, at least when a leader tip is out of the cloud. The runaway breakdown mechanism possibly works for upper atmosphere discharges [*Rakov and Uman*, 2003] but it demands quiet an extended high electric field region [*Gurevich et al.*, 2001]. So, the runaway breakdown is unrealizable for the case of space leaders because of insufficient streamer zone longitude which is no more than several dozens of meters [*Petersen and Beasley*, 2013]. Because of this there must be some fundamentally different mechanism responsible for the negative leader stepped development, which would allow ionization centers genesis in specific conditions of cold negative streamer corona devoid of any hydrometeors. In this work we introduce a new concept of space stem precursors formation at the negative corona streamer burst periphery. The proposed mechanism is based on noise-induced impact ionization provided by clusters of negative charge transferred into the negative corona volume together with negative streamer heads. One of the main results of this study is parameterization of space stem formation time as a function of an altitude above sea level h and spatiotemporal frequency of negatively charged streamer heads appearance inside the simulation domain

$$\eta = \frac{N_{str}}{Vt'}, \tag{1}$$

where N_{str} is a total number of streamers emanated from the negative leader tip and filling up the negative corona streamer burst with the volume V and lifetime t'. Note that parameter η together with the charge q_{str} concentrated inside the negative streamer head characterize the spatiotemporal noise intensity.

PROBLEM FORMULATION

The negative leader streamer zone is quiet complicated object with specific physical conditions. Unlike the case of relatively homogeneous positive leader streamer zone (see, for example, [*Raizer*, 2009]), the negative streamer corona description can't be reduced to the hemispherical shape and the constant electric field strength inside its volume. As it noted by *Gorin and Shkilev* [1976], who examined laboratory negative spark discharges development in long gaps, the negative leader streamer zone is strongly heterogeneous and consists of several distinctive highly structured negative streamer branches. Moreover, while it's commonly believed that the positive leader streamer zone develops continuously (although there are recent observations of steps in laboratory positive leader obtained by *Kostinskiy et al.* [2017]), the negative leader streamer corona exists in a form of streamer bursts finishing the step formation process, when quit a big amount of negative charge is distributed around the newly-formed negative leader tip. After each burst streamers of negative leader corona rapidly vanish until the next negative leader step, leaving negative space charge dispersed around a newly formed negative leader tip. There are numerous streamers simultaneously propagating inside the negative leader streamer zone during a negative corona streamer burst. Their negatively charged heads are conglomerations of electrons which practically lost electrical connection with the negative leader head [*Bazelyan and Raizer,* 2000]. Because of this, they can be treated as separate (but interacting with each other) clusters of negative charge propagating inside the negative corona space. There are wide spread of such characteristics as conductivities, electric currents, longitudinal electric fields, lengths, and radii of different negative streamer branches. It allows to consider the negative leader corona as a fractal system with fractal dimension concluded between 2 and 3. It was found by *Popov* [2002] that the positive streamer corona in 3-D case has the fractal dimension of $d_f^+ = 2.16$. As it was noted by *Gorin and Shkilev* [1976] that the negative leader streamer zone looks more scantily than the positive one, we conditionally consider that the negative corona streamer burst fractal dimension d_f^- is equal to 2.

In this study, we consider 0-12 km altitude range to analyze stem-formation process for both cloud-to-ground and cloud-to-air stepped leaders. Note that an ambient gas pressure p and temperature T_a [*Minyaev*, 2004] both depend on altitude above sea level h:

$$p\left[\mathrm{Torr}\right] = 760\exp\left(-\frac{h\left[\mathrm{km}\right]}{8.4}\right), \tag{2}$$

$$T_a\left[\mathrm{K}\right] = 288.15 - 6.49h[\mathrm{km}]. \tag{3}$$

In this study, we deal with 2-D numerical model. The simulation domain present rectangular parallelepiped (or a plane of a "unit thickness") divided into $100\times150\times1$ elementary cubic cells, which form a rectangular lattice. Since elementary cubes have faces of $2.5{\cdot}10^{-4}$ m, simulation domain has a volume of $V = 2.5{\cdot}10^{-2}\times3.75{\cdot}10^{-2}\times2.5{\cdot}10^{-4} = 2.34{\cdot}10^{-7}$ m^3 (note that cited values are given for ground level pressure and increase with height as described below). The model time step τ has an upper limit of 2.5 ns and can be diminished depending on the system state to ensure the calculation stability. The peculiarities of the simulation domain location and orientation are shown in Figure 1. The simulation domain is partly inside the negative leader streamer corona, while its bigger part is beyond the negative corona streamer burst volume (beyond the area available for negative streamer heads advancement). To reproduce all the peculiarities of the space stem formation process we consider special orientation of the model plane. The 2-D simulation domain is located in the same plane with the negative leader channel with *y*-axis directed along the ambient field $\overrightarrow{E_a} = E_a\overrightarrow{y_0}$ .and *x*-axis perpendicular to *y*-axis. This allows to study effects connected with electrons and ions drift along the ambient electric field direction, which are vital for the space stem-formation mechanism we propose.

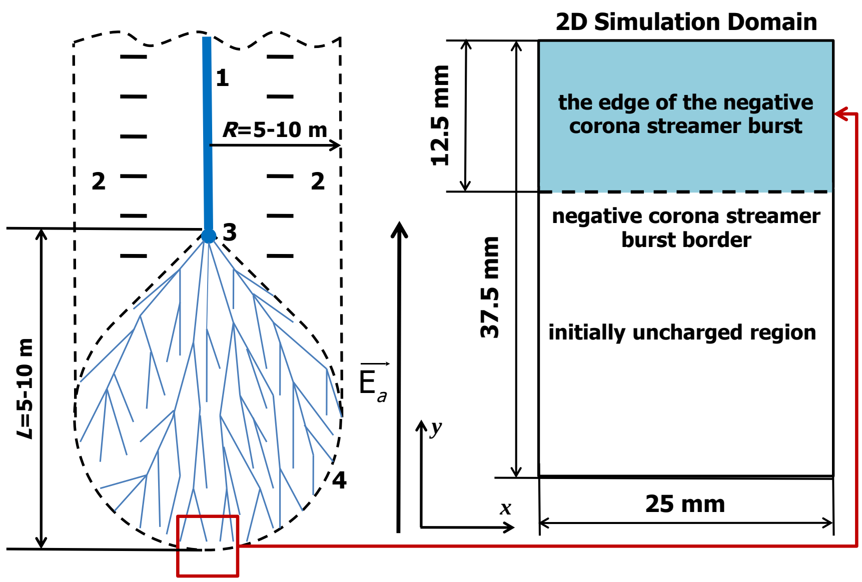

Figure 1. Simulation domain location and interior structure. The scheme shows (not to scale) (1) negative leader channel surrounded by (2) the negatively charged leader channel sheath with the radius *R* of about 5-10 m and ending with (3) the negative leader tip, which is the source of (4) the negative corona streamer burst with approximately the same radius and the extent *L* of about 5-10 m. The rectangular simulation domain with dimensions of 25 (along x-axis) and 37.5 (along y-axis) mm locates at the negative corona periphery, where an ambient electric field E_a is about 10 MV/m (see section 2), and divided into negatively charged region with the vertical extend of 12.5 mm (on the top) and uncharged region with the vertical extend of 25 mm (on the bottom). All the lengths and an ambient electric field magnitude are given here for ground level pressure (see text). Note that the space stem precursor formation occurs at the negative corona streamer burst border.

It's assumed that the simulation begins a little after the negative leader made a step, when first negative streamers reached the negative streamer corona periphery and begun to stop. Assuming the complexity of the negative corona streamer burst spatial structure, we locally define its periphery as an area of space at which negative streamers propagation stops. As soon as simulation begins, this part of simulation domain, which is inside the negative streamer corona, begins to fill up with spatially localized charges of negative streamer heads. There are $N_s = \eta V \tau$ streamers each time iteration invading the simulation domain, where model parameter η is spatiotemporal frequency of streamer heads appearance inside the considered volume. When they stop at different (random) grid nodes with $y \geq y_f$, where $y_f = 2.5$ cm is the outer boundary of the negative leader streamer corona (see Fig. 1), electron concentration locally increases by spatially distributed addition δn_e. As electric field strength decreases with increasing distance from the negative leader tip, we assume that streamers stop propagation when their heads enter the border, at which electric field strength becomes equal to negative streamer propagation field threshold varying with *h* as:

$$E^{-}_{pth}\left[\mathrm{MV/m}\right] = 1 \cdot \exp\left(-\frac{h\left[\mathrm{km}\right]}{8.4}\right). \tag{4}$$

Streamer head charges are assumed to be independent from *h*, while streamer head radii r^h_{str}, radii of streamer traces r^{tr}_{str}, and radii of streamer heating zones, according to similarity law *pd=const*, increase with height:

$$\left\{r^h_{str}, r^{tr}_{str}, r^T_{str}\right\} = \left\{r^h_{str0}, r^{tr}_{str0}, r^T_{str0}\right\}\frac{p\left(h=0\right)}{p\left(h\right)} = \left\{r^h_{str0}, r^{tr}_{str0}, r^T_{str0}\right\}\exp\left(\frac{h\left[\mathrm{km}\right]}{8.4}\right), \tag{5}$$

where specified radii r^h_{str0}, r^{tr}_{str0}, and r^T_{str0} at ground-level pressure are set to 0.1, 0.25, and 0.025 mm, respectively. In this model, the model grid spacing *a* is also obeys the dependence (5) with $a_0 = 2.5 \cdot 10^{-4}$ m to ensure the simulation similarity at various values of *h*. Streamer head charges are assumed to be distributed according to the following law:

$$q_{str}\left(\vec{r}, \vec{r_0}\right) = \frac{q^0_{str}}{2\pi r^{h\,2}_{str}} \cdot \begin{cases} \exp\left(\dfrac{\left(\vec{r}-\vec{r_0}\right)^2}{2\pi r^{h\,2}_{str}}\right), \; y < y_0 \\ \exp\left(\dfrac{\left(\vec{r_\perp}-\vec{r_{0\perp}}\right)^2}{2\pi r^{h\,2}_{str}} + \dfrac{z-z_0}{\lambda}\right), \; y \geq y_0 \end{cases}, \tag{6}$$

where q^0_{str} is a total streamer head charge, $\vec{r} = \{x; y\}$ and $\vec{r_0} = \{x_0; y_0\}$, where *x*-axis is oriented perpendicular to streamers propagation direction, which is co-directed with *y*-axis (see Fig 1), are radius-vectors of observation and streamer head center nodes, respectively. Characteristic distance of streamer charge decrease via electrons attachment to neutrals $\lambda = \mathrm{v}_{str}/\nu_{att}$ is determined as quotinent of streamer propagation speed v_{str} to attachment frequency ν_{att}. As we consider the situation, when streamers are going to stop, their speed must be close to the lowest possible value of 10^5 m/s [*Raizer*, 2009]. The attachment frequency ν_{att} is a function of reduced electric field $\xi = E/n_a$ (see the next section) given here for the breakdown condition, at which $E = E_b$, where $E_b = 3\cdot\exp\left(-h[\mathrm{km}]/8.4\right)$ MV/m is electric field of air breakdown, n_a is neutral molecules concentration. Relation (6) is close to streamer charge distribution used in [*Ivanovskiy*, 1996] and reflects the fact of the total streamer charge exponential decaying with increasing distance from its head. We assume that each streamer leaves a trail consisting of positive and negative ions and atomic oxygen, whose charge and concentrations, respectively, are described as:

$$q_n\left(\vec{r},\vec{r_0}\right) = q_p\left(\vec{r},\vec{r_0}\right) = \frac{\alpha q_{str}^0}{\left(2\pi r_{str}^{tr\,2}\right)^{d/2}}\cdot\exp\left(\frac{\left(\vec{r_\perp}-\vec{r_{0\perp}}\right)^2}{2r_{str}^{tr\,2}}\right)\times \quad ,\ \mathrm{y} > \mathrm{y}_0 \qquad (7)$$

$$\times\left(1-\exp\left(\frac{\mathrm{z}-\mathrm{z}_0}{\lambda}\right)\right)\cdot\frac{1}{1+\beta_{np}n_0\left(\mathrm{z}-\mathrm{z}_0\right)/\mathrm{v}_{str}}$$

$$n_O\left(\vec{r},\vec{r_0}\right) = \frac{\overline{n_O}}{\left(2\pi r_{str}^{h\,2}\right)^{d/2}}\cdot\begin{cases}\exp\left(-\frac{\left(\vec{r_\perp}-\vec{r_{\perp 0}}\right)}{2r_{str}^{h\,2}}\right), \mathrm{y}\ge y_0\\ \exp\left(-\frac{\left(\vec{r}-\vec{r_0}\right)}{2r_{str}^{h\,2}}\right), \mathrm{y} < y_0\end{cases}, \qquad (8)$$

where β_{np} are ion-ion recombination coefficient, $\overline{n_O} = 3\cdot 10^{21}\exp\left(-h[\mathrm{km}]/8.4\right)$ m^{-3} is the oxygen concentration value in the streamer core, $\alpha \approx 1/30$ is a coefficient, which reflects ions concentration reduction because of strong recombination occurring between electrons and positive ions at the streamer head. The last multiplier in relation (7) describes gradual reduction of ions concentration in the streamer trail via ion-ion recombination. Relation (8) assumes that each streamer head leaves behind a "streak" of atomic oxygen, whose concentration, neglecting dissipation, is assumed to be constant during the entire simulation time. Temperature increase, created by a streamer head is described as

$$T_{str}\left(\vec{r},\vec{r_0}\right) = \delta T\cdot\begin{cases}\exp\left(-\frac{\left(\vec{r_\perp}-\vec{r_{\perp 0}}\right)}{2r_{str}^{T\,2}}\right), \mathrm{y}\ge y_0\\ \exp\left(-\frac{\left(\vec{r}-\vec{r_0}\right)}{2r_{str}^{T\,2}}\right), \mathrm{y} < y_0\end{cases}, \qquad (9)$$

where $\delta T = 0.97$ K. Note that in our calculations we take into account the electric field created by streamer remnants only, neglecting the influence of still moving streamers. We don't consider the negative leader tip advancement, occurring at speed of about 10^4 m/s, because of both its relatively large distance from the simulation domain (a few dozens of meters) and small total simulation time (no more than about 2 μs).

The described spatial distribution of the negative streamer remnant, which is a basic element of spatiotemporal noise, is shown in Figure 2.

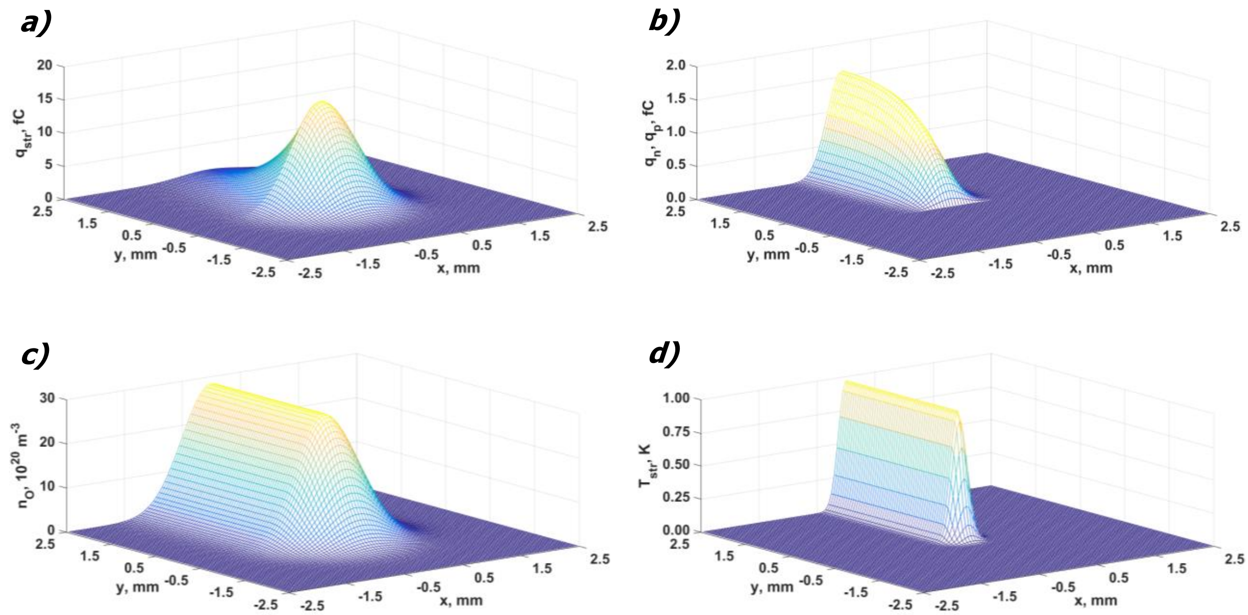

Figure 2. Spatial distribution of the negative streamer remnant, which acts as a basic element of spatiotemporal noise in our model, presented here for ground level pressure. Negative charge (a) is generally localized at the streamer remnant head and partially at its practically neutral trail consisting of (b) equal amount of positive and negative ions and (c) atomic oxygen. Temperature increase previously created by the streamer head is shown in section (d) of the figure. For higher altitudes the negative streamer remnant shape remains essentially the same, while its linear scale varies as $\exp\left(h[\mathrm{km}]/8.4\right)$.

To estimate the averaged over the negative corona streamer burst existence time t_b and its entire volume V_{sb} value of spatiotemporal frequency of streamer heads appearance at the streamer zone volume

$$\eta_a = \frac{N_{str}^{tot}}{V_{sb} t_b}, \tag{10}$$

where N_{str}^{tot} is the total number of streamers, stopping inside the streamer corona, one must take into account that the total amount of charge Q, which is throwed off from the negative leader tip during the negative corona streamer burst, has an order of magnitude of 1 mC. From the one hand, it can’t exceed 1-4 mC, which is the total charge transferred to the newly-formed lightning negative leader tip during the step formation process [*Rakov and Uman*, 2003]. From the other hand, the entire charge distributed in the negative leader corona can’t be significantly smaller than 1 mC, because the negative leader channel tip is too thin to hold a big charge. As a streamer head charge q_{str}^0 varies from 10^{-11} up to 10^{-9} C [*Bazelyan et al.*, 1975], a negative lightning leader head must emanate from 10^6 up to 10^8 streamers per each negative corona streamer burst. Assuming that streamers in air actively branch (see, for example, [*Popov*, 2002]), we suppose that stopping streamer heads went through multiple acts of division and, therefore, have minimum possible value of charge of 10^{-11} C (see discussion). So, we assume that each negative corona streamer burst distributes about 10^8 negative streamer heads in its volume. The temporal duration of the negative corona streamer burst t_b and the magnitude of the streamer corona volume V_{sb} are, generally speaking, vary with h. Since there are no any direct observations of these parameters, we can only designate the reasonable boundaries of their variation. As negative streamers participating in the negative corona streamer burst originate in intense electric field of strongly charged newly-formed negative leader tip, they first advance with near maximum speed of 10^7 m/s, slowing down only at the streamer zone periphery, where their speed falls to the minimum value of 10^5 m/s (see, for example, [*Raizer*, 2009]). So, one can assume that negative streamers propagate with the geometrically mean speed of 10^6 m/s, spreading over a typical for relatively small heights negative leader streamer corona longitude of about 5-10 m in t_b=5-10 μs, which may be taken for a minimum value of the negative corona formation time. Note that, according to similarity law *pd=const*, negative leader streamer zone longitude increase with altitude as p^{-1}. The upper bound of the negative corona streamer burst is the interstep time t_{is}, which is about 10-20 μs or more [*Rakov and Uman*, 2003; *Hill et al.*, 2011; *Petersen and Beasley*, 2013; *Qi Qi et al.*, 2016] for ground-level conditions and increases with height [*Rakov and Uman*, 2003]. As for the negative lightning leader streamer corona integral volume V_{sb}, which must sharply enlarge with height, we propose to estimate its ground value V_{sb}^0 as a volume of a cone with the height and the base radius of 10 m and 5 m, respectively, which is approximately equal to $V_{sb}^0 = 260$ m^3. Although it was noted by *Gorin and Shkilev* [1976] and *Kostinskiy et al.* [2017] that the negative corona of laboratory negative spark has nearly spherical form, high speed recording data obtained for natural lightning negative stepped leaders (see, for example, *Petersen and Baseley* [2013]) evidences that the negative leader corona is strongly elongated in the direction away from its tip and rather has a form close to paraboloid of revolution, which we for simplicity replace with a cone. This is probably because lightning leader develops in upward ambient electric field and has charged leader channel sheath, joint action of which distorts negative corona form pushing negative streamers in the direction of negative leader advancement. Since negative streamer zone can be considered as a fractal system, its real volume depends on the fractal dimension $d_f^- = 2$. Assuming that the streamer corona volume increases with increasing height as p^{-3}, one can conclude that

$$V_{sb}\left[\mathrm{m}^3\right] = V_{sb}^{0\,\frac{d_f^-}{3}} \cdot \exp\left(3h\left[\mathrm{km}\right]/8.4\right) \approx 40 \cdot \exp\left(3h\left[\mathrm{km}\right]/8.4\right). \tag{11}$$

So, assuming that $t_b = (5-20)\cdot \exp\left(h\left[\mathrm{km}\right]/8.4\right)$ μs, we can designate the value of ambient spatiotemporal frequency of streamer heads appearance inside negative corona volume as

$$\eta_a\left[\mathrm{m}^{-3}\cdot \mathrm{s}^{-1}\right] = \frac{Q}{q_{str}^0 V_{sb} t_b} \cdot \exp\left(-4h\left[\mathrm{km}\right]/8.4\right) \approx 10^{11} \cdot \exp\left(-4h\left[\mathrm{km}\right]/8.4\right). \tag{12}$$

Relation (12) demonstrates that the magnitude of η_a rapidly decrease with increasing altitude above sea level h. Note that the relation (12) gives only conditional estimation of the magnitude of η_a, while its real value can significantly vary from one negative streamer burst to another even for the same altitude above sea level *h*.

It should be noted that at the beginning, when electric field of the negative leader head isn't shielded by the negative corona space charge, there must be larger quantity of negative streamer heads at the negative corona periphery (where we place our simulation domain). This is because propagating streamers aren't yet affected by the locking charge of previously emanating streamers and propagate to the very border of the negative corona streamer burst.

MODEL EQUATIONS

To examine the processes inside the negative leader streamer zone we consider the following system of differential equations describing the spatiotemporal evolution of electron and positive and negative ions concentrations n_e, n_p, and n_n, respectively:

$$\begin{cases} \dfrac{\partial n_e}{\partial t} + div\overrightarrow{J_e} = \left(\nu_i - \nu_{att}\right) n_e + \nu_{dett} n_n - \beta_{ep} n_e n_p + f\left(\vec{r}, t\right) + \Omega & (13.1) \\ \dfrac{\partial n_p}{\partial t} + div\overrightarrow{J_p} = \nu_i n_e - \beta_{ep} n_e n_p - \beta_{np} n_n n_p + \Omega & (13.2) \\ \dfrac{\partial n_n}{\partial t} + div\overrightarrow{J_n} = \nu_{dett} n_n + \nu_{att} n_e - \beta_{np} n_n n_p & (13.3) \end{cases}$$

with typical for atmospheric air at ground pressure [*Raizer*, 2009] initial values $n_e^0 = 10^4$ m^{-3}, $n_n^0 = n_p^0 = 10^9$ m^{-3}, where ν_i, ν_{att}, and ν_{dett} are ionization, attachment and detachment frequencies, respectively; β_{ep} and β_{np} are electron-ion and ion-ion recombination coefficients; $\Omega = 10^7$ m^{-3}/s [*Raizer*, 2009] is the number of pairs of electrons and positive ions, created by collisions or ionization of neutrals by photons and cosmic particles in a unitary volume per unit time; $\overrightarrow{J_e}$, $\overrightarrow{J_n}$, and $\overrightarrow{J_p}$ are electron and positive and negative ions flux densities respectively;

$$f\left(\vec{r}, t\right) = \sum_{i=1}^{N_{str}} \frac{q_{str}\left(\vec{r}, \overrightarrow{r_{0i}}\right)}{e\tau} \theta\left(t, t_{stop}^i\right) \qquad (14)$$

is spatiotemporal noise, associated with additional charges of just stopped negative streamer heads, where $e = -1.6 \cdot 10^{-19}$ C is the electron charge. The index *i* in formula (14) denotes a streamer head, stopped at the node with the radius-vector $\overrightarrow{r_{0i}}$, N_{str} is a total number of streamers invading the modeling area during the entire simulation time. Function $\theta\left(t, t_{stop}^i\right)$ is equal to one if $t = t_{stop}^i$ and is equal to zero otherwise, where t_{stop}^i is a moment of discrete modeling time, multiple of 2.5 ns and corresponding to *i*-th streamer head stopping. As in this model we neglect the influence of still moving streamers, the system of equations (13) describes only the evolution of streamer remnants. In relation to the charge conservation law, we must note that the total charge in the model system is a sum of charges of individual streamer heads entering the simulation domain. Corresponding flux densities can be found as

$$\begin{cases} \overrightarrow{J_e} = -\mu_e n_e \vec{E} - D_e \nabla n_e & (15.1) \\ \overrightarrow{J_n} = -\mu_n n_n \vec{E} - D_n \nabla n_n & (15.2) \\ \overrightarrow{J_p} = \mu_p n_p \vec{E} - D_p \nabla n_p, & (15.3) \end{cases}$$

where μ_e, μ_n, and μ_p are electron and negative and positive ions mobilities respectively, D_e, D_n and D_p are electron and negative and positive ions diffusion coefficients, respectively. Electrical potential φ is created by charges located at the spatial grid nodes and can be found as the solution of Poisson's equation. In this study, the potential is calculated using the following relation:

$$\varphi(\vec{r}) = \frac{1}{4\pi\varepsilon_0}\left(\sum_{\vec{r}' \neq \vec{r}} \frac{q(\vec{r}')}{\left|\vec{r} - \vec{r}'\right|} + \frac{q(\vec{r})}{a/2}\right) + \varphi_0, \qquad (16)$$

where $q(\vec{r})$ and $q(\vec{r}')$ are charges located at space-grid nodes with radius vectors $\vec{r} = \{x, y\}$ (observation point; the last term in the parentheses) and $\vec{r}' = \{x', y'\}$ (source points; the first term in the parentheses), respectively, $\varepsilon_0 = 8.85 \cdot 10^{-12}$ F/m is the electric permittivity of vacuum, a is the grid spacing, $\varphi_0 = -E_a \overrightarrow{y_0}$ is the background potential. Electrical charge at the space-grid node with radius vector $\vec{r}$ is specified as

$$q(\vec{r}) = -e\left(n_p(\vec{r}) - n_e(\vec{r}) - n_n(\vec{r})\right)a^3. \qquad (17)$$

The electric field $\vec{E}$ can be found as

$$\vec{E} = -\nabla\varphi. \qquad (18)$$

The boundary conditions we use to calculate the potential (16) and electric field (18) is visualized in Figure 3. It's assumed that the simulation domain is surrounded by 8 rectangular areas with different dimensions selected so that the calculation correctness is ensured. Each of this auxiliary regions is filled with space charges, which present the mirror reflection of space charges located at the simulation domain in the border between the latter and the specified additional area. Thus, each charge in the simulation domain has 8 equal to it and to each other reflections, 4 of which correspond to reflections in simulation rectangular borders and 4 others correspond to its vertexes (as if the simulation domain would be enclosed between 4 vertically oriented flat mirrors). Space charge of these additional areas contributes the potential (16), which allows to avoid the presence of unjustifiedly increased electric field at the simulation domain borders, where the space charge experiences a sharp jump to zero level. As this approach involves only charges obtained in the model realization without resorting to, for example, applying of their random values, we consider the use of such kind of boundary conditions as the most natural way to describe the potential distribution over the simulation domain.

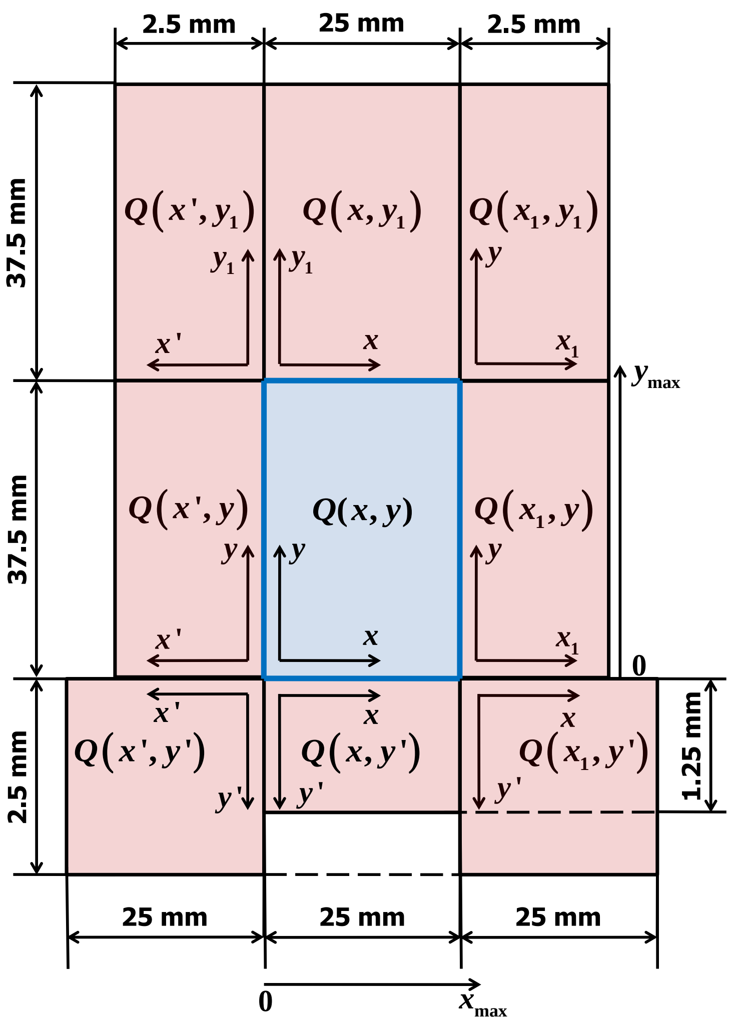

Figure 3. Boundary conditions implemented in the model to provide the correctness of electric potential calculation. The simulation and auxiliary domains with specified dimensions, which was experimentally selected to ensure the potential calculation correctness, are shown in blue and pink, respectively. Supplementary space charge encircling the modeling area (virtual charge) is defined as a mirror reflection of the charge inside the simulation domain (charge produced during the model realization) in 4 borders and 4 vertexes of simulation rectangular (as if it is enclosed between 4 vertically oriented flat mirrors shown by bold blue line segments), that is $x' = -x$, $y' = -y$, $x_1 = x_{\max} - x$, and $y_1 = y_{\max} - y$.

Divergences of corresponding flux densities (15) can be found as

$$\begin{cases} div\overrightarrow{J_e} = div\left(n_e \overrightarrow{v_e}\right) - D_e \nabla^2 n_e - \nabla D_e \cdot \nabla n_e & (19.1) \\ div\overrightarrow{J_n} = div\left(n_n \overrightarrow{v_n}\right) - D_n \nabla^2 n_n - \nabla D_n \cdot \nabla n_n & (19.2) \\ div\overrightarrow{J_p} = div\left(n_p \overrightarrow{v_p}\right) - D_p \nabla^2 n_p - \nabla D_p \cdot \nabla n_p, & (19.3) \end{cases}$$

where $\overrightarrow{v_e} = -\mu_e \vec{E}$, $\overrightarrow{v_p} = \mu_p \vec{E}$, and $\overrightarrow{v_n} = -\mu_n \vec{E}$ are electron and positive and negative ions drift velocities, respectively.

As electron and positive and negative ions mobilities and ion-ion recombination rate are inversely proportional to gas pressure p [*Raizer*, 1991], according to relation (2), we assume that

$$\begin{cases} \mu_e\left[\dfrac{m^2}{V\cdot s}\right]=5.92\cdot 10^{-2}\exp\left(\dfrac{h[\mathrm{km}]}{8.4}\right) & (20.1)\\ \mu_p\left[\dfrac{m^2}{V\cdot s}\right]=1.37\cdot 10^{-4}\exp\left(\dfrac{h[\mathrm{km}]}{8.4}\right) & (20.2)\\ \mu_p\left[\dfrac{m^2}{V\cdot s}\right]=1.51\cdot 10^{-4}\exp\left(\dfrac{h[\mathrm{km}]}{8.4}\right) & (20.3)\\ \beta_{np}\left[\dfrac{m^3}{s}\right]=10^{-13}\exp\left(\dfrac{h[\mathrm{km}]}{8.4}\right). & (20.4)\end{cases}$$

In the present work we consider the ionization ν_i and attachment ν_{att} frequencies as the following functions of reduced electric field $\xi=(E/n_a)\cdot 10^{16}$ V·cm^2:

$$\nu_i(\xi)=n_a\left(0.8k_5(\xi)+0.2k_6(\xi)\right), \tag{21}$$

$$\nu_{att}(\xi)=0.2n_a k_9(\xi), \tag{22}$$

where n_a is the neutrals concentration in units of cm^{-3}, and the dependence of rate constants $k_5(\xi)$, $k_6(\xi)$, and $k_9(\xi)$ on ξ are given in Table 1. Electron-ion recombination coefficient is assumed to be a function of electron temperature T_e:

$$\beta_{ep}=2\cdot 10^{-10}\left(\frac{300}{T_e[K]}\right). \tag{23}$$

According to *Belinov and Naidis* [2003], T_e depends on reduced electric field:

$$T_e[\mathrm{eV}]=\begin{cases} 0.447\left(\dfrac{E}{n_a}[\mathrm{Td}]\right)^{0.16}, & \dfrac{E}{n_a}[\mathrm{Td}]<50\\ 0.0167\dfrac{E}{n_a}[\mathrm{Td}], & \dfrac{E}{n_a}[\mathrm{Td}]>50.\end{cases} \tag{24}$$

The detachment frequency ν_{dett} can be found as

$$\nu_{det}=3\cdot 10^{-16}n_a\left[m^{-3}\right]n_O\left[m^{-3}\right], \tag{25}$$

where atomic oxygen concentration n_O obeys the following equation:

$$\frac{dn_O}{dt}=2n_e n_{O_2}k_{diss}^{eff}-6\cdot 10^{-34}\left(\frac{300}{T_g}\right)^2 n_O n_{O_2} n_a+\frac{\delta n_O(\vec{r},t)}{\tau} \tag{26}$$

with initial condition $n_O(t=0)=0$, where T_g is local gas temperature, molecular oxygen concentration n_{O_2} in atmospheric air, which can be treated as N_2:O_2=4:1 mixture, is equal to $0.2n_a$, the effective oxygen dissociation constant k_{diss}^{eff} can be calculated via rate constants from Table 1 as:

$$k_{diss}^{eff} = 4\left(k_1(\xi)+k_2(\xi)+k_3(\xi)+k_4(\xi)+k_5(\xi)\right)+k_6(\xi)+k_7(\xi)+k_8(\xi). \quad (27)$$

Table 1. The rate constants of some electronic processes in N_2:O_2 = 4:1 mixture as functions of the reduced electric field $\xi=(E/N)\cdot 10^{16}$ V·cm^2: $log_{10}(k)=A+B/\xi$ (the rate constants k and k* are in units of cm^3/s).

№	Reaction	*A*	*B*	ξ
1	$e + N_2 \rightarrow N_2(A^3\Sigma_u^+) + e$	-8.4	-17.11	2-10
1^*	$e + N_2 \rightarrow N_2(A^3\Sigma_u^+) + e$	-8.67	-14.4	10-100
2	$e + N_2 \rightarrow N_2(B^3\Pi_g) + e$	-7.91	-16.81	2-10
2^*	$e + N_2 \rightarrow N_2(B^3\Pi_g) + e$	-8.2	-13.92	10-100
3	$e + N_2 \rightarrow N_2(a^1\Pi_g) + e$	-8.17	-18.74	3-10
3^*	$e + N_2 \rightarrow N_2(a^1\Pi_g) + e$	-8.29	-17.53	10-100
4	$e + N_2 \rightarrow N_2(C^3\Pi_u) + e$	-7.88	-23.32	4-20
4^*	$e + N_2 \rightarrow N_2(C^3\Pi_u) + e$	-8.08	-19.37	20-100
5	$e + N_2 \rightarrow N_2^+ + 2\cdot e$	-8.09	-40.29	8-30
5^*	$e + N_2 \rightarrow N_2^+ + 2\cdot e$	-7.37	-61.81	30-100
6	$e + O_2 \rightarrow O_2^+ + 2\cdot e$	-8.31	-28.57	6-26
6^*	$e + O_2 \rightarrow O_2^+ + 2\cdot e$ (see below)	-	-	-
7	$e + O_2 \rightarrow O(^3P) + O(^3P) + e$	-7.78	-14.08	3-10
7^*	$e + O_2 \rightarrow O(^3P) + O(^3P) + e$	-8.31	-8.78	10-30
7^{**}	$e + O_2 \rightarrow O(^3P) + O(^3P) + e$	-8.6	0.	30-100
8	$e + O_2 \rightarrow O(^3P) + O(^1D) + e$	-7.43	-17.06	3-10
8^*	$e + O_2 \rightarrow O(^3P) + O(^1D) + e$	-7.6	-15.43	10-100
9	$e + O_2 \rightarrow O^- + O$	-9.42	-12.7	3-9
9^*	$e + O_2 \rightarrow O^- + O$	-10.21	-5.7	9-30

(6^*) $k_{ion}=10^{-7.54-48.57/\xi}\cdot(1+4\cdot 10^{-7}\cdot\xi^3)$, ξ=26-100.

Atomic oxygen concentration addition worked-out by heads of negative streamers, each of which carry an intensive electric field, is

$$\delta n_O\left(\vec{r},t\right)=\sum_{i=1}^{N_{str}} n_O\left(\vec{r},\overrightarrow{r_{0i}}\right)\theta\left(t,t_i\right). \tag{28}$$

Assuming the Maxwellian energy spectrum of electrons and ions we use diffusion coefficients expressions arising from the Einstein relation:

$$\begin{cases} D_e=\dfrac{\mu_e k_B T_g}{e} & (29.1)\\ D_n=\dfrac{\mu_n k_B T_g}{e} & (29.2)\\ D_p=\dfrac{\mu_p k_B T_g}{e}, & (29.3)\end{cases}$$

where k_B is the Boltzmann's constant.

To describe the local gas temperature T_g evolution one must take into account both Joule gas heating and the vibrational nitrogen states relaxation. So, we assume that temperature evolution obeys the following equation:

$$\frac{dT_g}{dt}=\frac{2}{7n_a k_B}\left[\left(1-f_V\right)jE+\frac{\varepsilon_V(T_V)-\varepsilon_V(T_g)}{\tau_{VT}}\right]+D_T\nabla^2 T_g \tag{30}$$

with initial condition $T_g\left(t=0\right)=T_a$, where current density

$$\vec{j}=\left|e\right|\left(\mu_e n_e+\mu_p n_p+\mu_n n_n\right)\vec{E}, \tag{31}$$

f_V=0.95 is the fractions of the Joule energy transferred to the molecules in the form of vibrational excitation,

$$\varepsilon_V(T_V)=n_a\frac{\varepsilon_{V=1}}{\exp\left(\varepsilon_V/\left(k_B T_V\right)\right)-1} \tag{32}$$

is vibrational energy density, where $\varepsilon_{V=1}$=0.28 eV is the energy of the first exited vibrational state of N_2 molecule, T_V is vibrational temperature, τ_{VT} is characteristic time of vibrational excitation relaxation, D_T is the thermal diffusivity coefficient, which varies with the gas temperature T_g acording to the following law

$$D_T\left[\frac{m^2}{s}\right]=\begin{cases}1.9\cdot 10^{-5}+0.01761\left(\dfrac{T_g\left[K\right]}{273}-1\right), & T_g<400\text{ K}\\ 2.92\cdot 10^{-3}+0.0115\left(\dfrac{T_g\left[K\right]}{273}-1\right), & T_g\geq 400\text{ K.}\end{cases} \tag{33}$$

Vibrational energy reservoir is pumped up with the Joule energy and decreases because of relaxation in accordance with the following equation

$$\frac{d\varepsilon_V(T_V)}{dt} = f_V\, jE - \frac{\varepsilon_V(T_V) - \varepsilon_V(T_g)}{\tau_{VT}} \tag{34}$$

with initial condition $\varepsilon_V\left(t=0\right) = \varepsilon_V\left(T_a\right)$, where vibrational excitation relaxation time τ_{VT} is a function of atomic oxygen n_O and ozone n_{O_3} concentrations:

$$\tau_{VT} = \frac{1}{k_O n_O + k_{O_3} n_{O_3}}, \tag{35}$$

where corresponding rate constants $k_O = 4.5\cdot 10^{-15}\left(T_g/300\right)^{2.1}$ cm^3/s, $k_{O_3} = 5\cdot 10^{-14}$ cm^3/s. Ozone number density n_{O_3} evolution obeys the following equation

$$\frac{d}{dt} n_{O_3} = n_O \cdot n_{O_2} \cdot n_a \cdot k_{O-O_3} \tag{36}$$

with initial condition $n_{O_3}\left(t=0\right) = 0$, where the rate constant $k_{O-O_3} = 6.2\cdot 10^{-34}$ cm^3/s.

In this work we assume that system evolves too slowly to alter the gas pressure p. Because of this neutrals concentration n_a varies with gas temperature as

$$n_a = n_a^0\left(\frac{T_g}{T_a}\right), \tag{37}$$

where initial gas concentration $n_a^0 = 2.7\cdot 10^{25}\left(p\left[\mathrm{Torr}\right]/760\right)\cdot\left(273/T_g\left[\mathrm{K}\right]\right)$ m^{-3}.

Note that in this work we solve the following system of evolutionary equations (13), (26), (30), (34), and (36) reduced to the following recurrent form:

$$\left\{\begin{array}{ll}
\widetilde{n_e}\,|_{t+\tau} = \widetilde{n_e}\,|_t + \tau\left[\left(\nu_i - \nu_{att} - \beta_{ep} n_0 \widetilde{n_p}\,|_t + D_e\nabla^2 + \nabla \mathrm{D_e} \nabla\right)\widetilde{n_e}\,|_t - div\left(\widetilde{n_e}\,|_t\, \overrightarrow{\mathrm{v}_e}\right) + \nu_{det}\widetilde{n_n}\,|_t + \frac{\Omega}{n_0} + \frac{f\left(\vec{r},t\right)}{n_0}\right] & (38.1)\\
\widetilde{n_p}\,|_{t+\tau} = \widetilde{n_p}\,|_t + \tau\left[\left(-\beta_{ep} n_0 \widetilde{n_e}\,|_t - \beta_{np} n_0 \widetilde{n_n}\,|_t + D_p\nabla^2 + \nabla \mathrm{D}_i \nabla\right)\widetilde{\mathrm{n}_p}\,|_t - div\left(\widetilde{n_p}\,|_t\, \overrightarrow{\mathrm{v}_p}\right) + \nu_i \widetilde{n_e}\,|_t + \frac{\Omega}{n_0}\right] & (38.2)\\
\widetilde{n_n}\,|_{t+\tau} = \widetilde{n_p}\,|_t + \tau\left[\left(-\nu_{det} - \beta_{np} n_0 \widetilde{n_p}\,|_t + D_n\nabla^2 + \nabla \mathrm{D}_i \nabla\right)\widetilde{n_n}\,|_t - div\left(\widetilde{n_n}\,|_t\, \overrightarrow{\mathrm{v}_n}\right) + \nu_{att}\widetilde{n_e}\,|_t\right] & (38.3)\\
\widetilde{n_O}\,|_{t+\tau} = \widetilde{n_O}\,|_t + \tau\left(2\widetilde{n_e}\widetilde{n_{O_2}} n_0 k_{diss}^{eff} - 6\times 10^{-34} n_0 \left(\frac{300}{T_g\,|_t}\right)^2 \widetilde{n_O}\widetilde{n_{O_2}} n_a\right) + \delta\widetilde{n_O}\left(\vec{r},t\right) & (38.4)\\
T_g\,|_{t+\tau} = T_g\,|_t + \tau\left[\frac{2}{7 n_a k_B}\left[\left(1 - f_V\right) jE + \frac{\varepsilon_V(T_V)\,|_t - \varepsilon_V(T_g\,|_t)}{\tau_{VT}}\right] + D_T\left(T_g\,|_t\right)\nabla^2 T_g\,|_t\right] & (38.5)\\
\varepsilon_V(T_V)\,|_{t+\tau} = \varepsilon_V(T_V)\,|_t + \tau\, f_V\, jE - \frac{\varepsilon_V(T_V)\,|_t - \varepsilon_V(T_g\,|_t)}{\tau_{VT}} & (38.6)\\
\widetilde{n_{O_3}}\,|_{t+\tau} = \widetilde{n_{O_3}}\,|_t + \tau\widetilde{n_O}\cdot\widetilde{n_{O_2}}\cdot n_a \cdot n_0 k_{O-O_3}, & (38.7)
\end{array}\right.$$

where upper wave symbol denotes dimensionless concentrations normalized to the value n_0=10^{20} m^{-3}. Initial values of concentrations in these equations are also normalized to n_0.

In this work we use proposed model to simulate the stem formation process and study how the stem formation time depends on parameter η at different altitudes above sea level h.

RESULTS

The space stem formation process we model develops in several stages schematically shown in Figure 4. The simulation finishes with the formation of positively charged cluster of positive ions, which peak charge value exceeds the established threshold $q_{th}^{+} = 2 \cdot 10^{-11}$ C. The further processes, which are connected with a positive streamer initiation on the base of the previously formed positively charged cluster, are discussed but aren't modeled in this study.

Stopping negative streamer head is a cluster of negative charge (see Fig. 2a), which creates an electric field peak localized on the scale of a streamer head radius r_{str}^{h}. Although each negative streamer head remnant is a center of increased ionization, the charge of a single negative streamer remnant can't trigger the breakdown process by itself because the ionization frequency ν_i it can provide is much less than the attachment one ν_{att}. To run the space stem formation process one needs the simultaneous presence of multiple negative streamer remnants, charges of which contribute spatiotemporal noise. The intensity of this noise is defined by the spatiotemporal frequency of streamer appearance η. When a relatively big amount of stopped negative streamer heads get in the same area during a short period of time (see stage A in Fig. 4), collective action of their negative charge can locally produce electric field, which is strong enough to create an ionization center, that is a domain of space at which the ionization rate exceeds the attachment one (see stage B in Fig. 4). Note that ionization centers always form at the negative corona streamer burst periphery, where the ambient electric field is intensified by the field created by the negative space charge of streamer heads remnants. Such centers produce both electrons and positive ions (see stage C in Fig. 4). Although the number densities of generated electrons and positive ions decrease because of recombination and attachment processes, there is the separation of positive and negative charge carriers provided with their drifting in local electric field (see stage D in Fig. 4). Since electrons mobility is at least two orders of magnitude greater than that of positive ions, free electrons produced at the ionization center periphery rush against the local field direction, leaving behind positively charged spot. As strong electric field, in which intensive ionization takes place, is provided with electrons charge, there occurs ionization wave advancing against the ambient electric field direction and leaving behind a positively charged trace consisting of positive ions and significantly smaller amount of negative ones (see stages E and F in Fig. 4). As the most intensive drifting takes place at the ionization center lower bound (which corresponds to smaller ordinate in our model (see Fig. 1)), where both electric field and electron concentration gradient are maximal, the main part of newly produced electrons overlap the previously existing ones (those, which launched the ionization center formation or were produced by the ionization center up to the specified moment of time), while the rest (insignificant part) of worked-out electrons, which are closer to the negative leader tip (which have bigger ordinate in our model (see Fig. 1)), fall behind the ionization wave front and either recombine with positive ions or transform into negative ones because of attachment to neutral molecules at the positively charged ionization wave trail. The negative charge permanent accumulation, taking place at the ionization wave front, locally amplifies electric field and, consequently, the capability of producing new electrons and positive ions and so on. So, there is a kind of positive feedback, which provides bigger and bigger positive ions concentration at each new ionization wave front position. Finally, there comes a moment when many times amplified ionization wave generates a positively charged cluster with the peak charge exceeding the established threshold of $2\cdot10^{-11}$ C coexisting with the negatively charged cluster with the bigger absolute charge located at the ionization wave front (see stage F in Fig. 4). We assume that the resulting dipole structure with an excess of negative charges is a space stem precursor. So, we state that positively charged domain playing the role of floating anode in the positive streamer initiation process forms as a result of relatively big negative charge concentration occurring in a negligibly small area of space in a very short time.

As soon as the needful domain of positive ions is formed, we are waiting for the Meek's criterion fulfillment:

$$\frac{\nu_i-\nu_{att}}{\mathrm{v}_{dr}}x\geq\frac{22}{\ln\left(\overline{n_e}\right)}, \tag{39}$$

where x is the length of line segment traveled by an evolving electron avalanche against the local electric field orientation, $\overline{n_e}$ is free electrons ambient concentration,

$$\mathrm{v}_{dr}\left(\zeta\right)[\text{m/s}]=-7.36\cdot10^{-5}\zeta^4+5.11\cdot10^{-2}\zeta^3-12\zeta^2+2.02\cdot10^3\zeta+4.92\cdot10^3 \tag{40}$$

is the electrons drift velocity, which was parameterized based on experimental data provided by *Dutton* [1975], where ζ is reduced electric field in Td.

As in our model we for simplicity assume that the increased level of spatiotemporal frequency of streamer head appearance takes place over the entire simulation domain volume, which seems to be an unlikely case, free electrons ambient concentration $\overline{n_e}$ facilitating Meek's criterion fulfillment must be estimated as an average value over the entire negative corona streamer burst volume $\overline{n_e}=Q/\left(eV_{sb}\right)=10^{14}$ m^{-3}.

We assume that a positive streamer can be formed via an avalanche to streamer transition if an electron avalanche, for which the Meek's criterion has already been met, pours into a positively charged domain, the charge of which is sufficient to ensure a positive streamer initiation. Actually, a bidirectional streamer may form because of the presence of big negative charge at the ionization wave front (see stage G in Fig. 4). Note that the established threshold value $q_{th}^{+}=2\cdot10^{-11}$ C is comparable with the minimal streamer head charge being of 10^{-11} C. So, we use previously formed positively charged domain as a floating anode needed for positive streamer initiation. This concept coincides with the space streamer initiation and propagation mechanism described by *Les Renardieres group* [1981]. Note that, as the magnitude of the model positive charge peak value is averaged over the spatial grid step, its actual value can be bigger.

Despite positive ions spot is surrounded by the negative charge, it can survive for a relatively long time, which is enough to form a positive streamer. At first, as the lion share of generated electrons groups at the ionization wave front, the ionization wave trace is positively charged. At second, recombination process occurring between positive and negative ions at the ionization wave trace (we neglect free electrons because they either recombined with positive ions or attached to neutrals turning into the form of negative ions) is slowed down because "sedentary" ions close very slowly compared to the criterion (39) fulfillment.

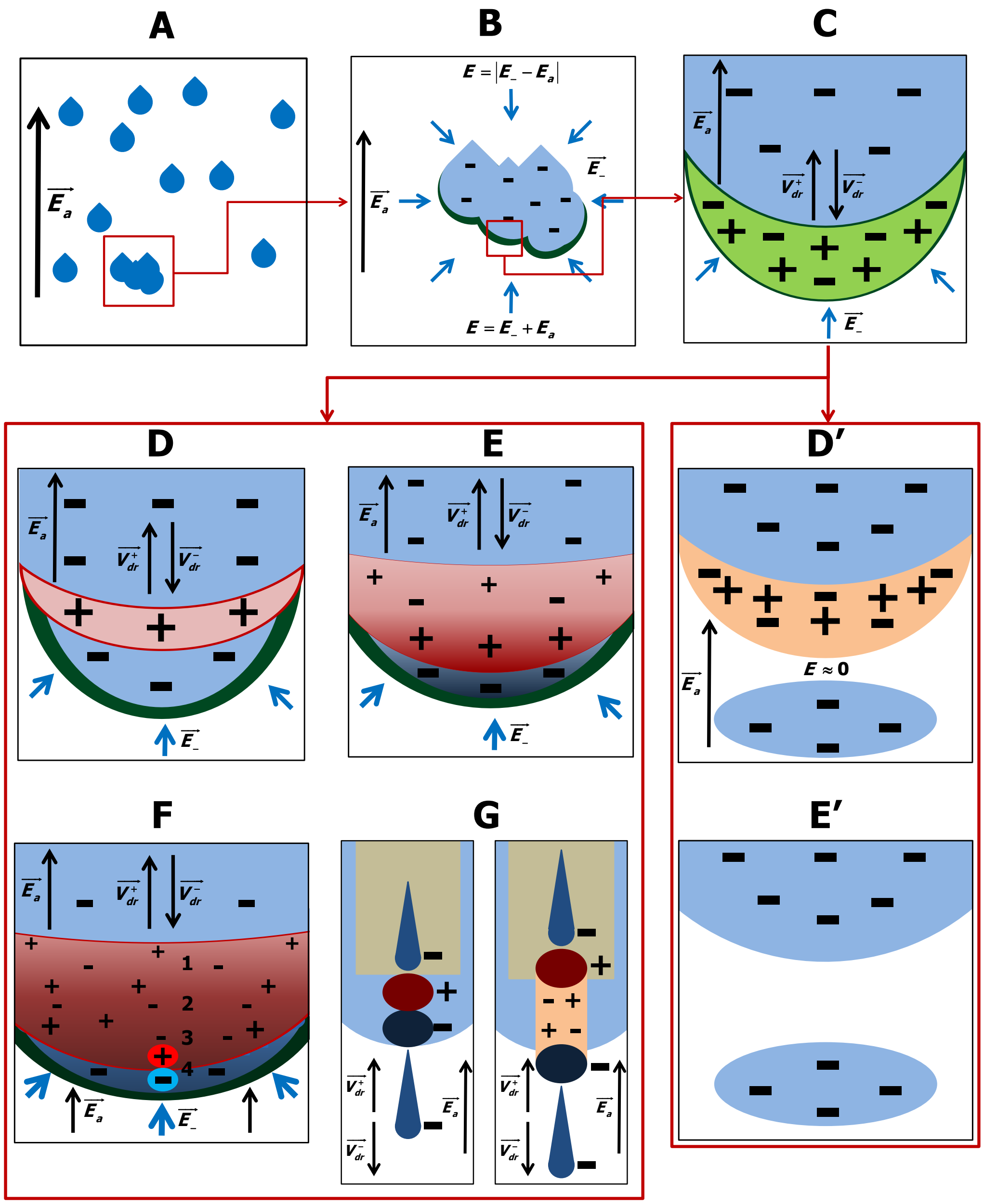

Fig. 4. Space stem precursor formation scheme (see sec. 4). (A) Several stopped negative streamer heads (shown by blue droplets) get into the same area of space forming negatively charged domain and locally increasing the electric field up to the breakdown value E_b. (B) Qualitative electric field distribution scheme showing its intensification at the negatively charged domain outer border (this one which is farther from the negative leader tip), where electric field of space charge $\vec{E_-}$ (shown by blue arrows) is co-directed with the ambient one $\vec{E_a}$ (shown by the black arrow). That is, ionization bound (shown in dark-green) arises at which ionization frequency exceeds the attachment one. (C) Ionization bound (shown in green) generates equal amount of electrons and positive ions subjected to drifting in intense local

electric field. (D) Free electrons quickly move against the local electric field baring positive ions and forming the dipole layer: the ionization wave front shifts. (E) Repetition of processes (C) and (D) leads to the elongation of the positive trace created by the ionization wave front. Note that the number of free electrons and, consequently, the ionization bound intensity increases as the ionization wave advances (see text). (F) Ionization wave enhancement and advancement continues until the formation of positive ions domain (shown by red oval) with the peak charge value exceeding the established threshold of $2 \cdot 10^{-11}$ C, which coexists with the oppositely charged electrons domain (shown by blue oval) having bigger absolute charge magnitude. We consider resulting dipole structure with an excess of negative charge as a space stem precursor. Note that positive ions concentrations increase from one ionization bound position to another (they are numerated from 1 to 4) because of its intensification, that is, $n_{p1}<n_{p2}<n_{p3}<n_{p4}$ (G). Positive and negative domains works as floating electrodes launching electron avalanches (shown by dark-blue conical structure) formation and, consequently, bidirectional streamer propagation, the plasma channel of which is shown by light orange. Note that the positive streamers get into the region with favorable conditions (see Fig. 5(IV)), which is shown in grey, and that simulation of this stage is beyond the scope of the present study. Stages (A)-(G) correspond to space stem precursor successful formation, while stages (D') and (E') correspond to one of possible scenarios of its dying out. (D') Ionization wave stumbles upon the negatively charged domain. This leads to electric field reduction at the ionization wave front, which stops both ionization and drifting and facilitates electron-ion recombination (recombination zone is shown in beige). (E') Ionization wave decays.

The described sequence of processes demands the presence of permanent strong electric field at the ionization center periphery. This condition can be fulfilled only if electric field produced by the ionization center negative space charge is co-directed with an ambient one. If the ionization wave front gets into weak local electric field, it rather decays. For example, the ionization wave can stumble upon negatively charged area (see stages D' and F' in Fig. 4), which abundantly fill the negative corona streamer burst volume. This fact once again emphasizes the role of the negative corona periphery in the space stem formation process.

Simulations show that the ionization wave can also decays by itself in the following way. Electric field at the ionization wave front contributes its inflation: the ionization bound radius of curvature permanently increases because of Coulomb repulsion occurring between electrons. If, for some reasons, the rate of electrons spreading out increases the rate of their production because of ionization, ionization wave gradually disappears. So, the ionization wave development depends on many factors and only part of them can lead to space stem precursor formation.

An example of simulation obtained for the ground level pressure is shown if Figure 5 (I-III), which demonstrates initial, middle and final stages of space stem precursor formation process.

It's important to note that Meek's criterion can be met without the presence of any positively charged domains. But in this case only a negative streamer can be produced, which advances beyond the borders of the negative corona streamer burst and quickly stops propagation because of low ambient electric field magnitude, which is insufficient to support negative streamer propagation. Positive streamers, on the contrary, when approaching the negative leader tip, enter the area of constant (on the average) electric field $E_a = 10^6$ V/m, which is twice as large as minimal electric field needed for positive streamers stable propagation $E_{pth}^{+} = 5 \cdot 10^{5}$ V/m (see, for example, *Raizer* [2009]). Moreover, positive streamers, emanated from space stem, advances under favorable conditions of increased (1) electron number density, (2) detachment frequency, and (3) gas temperature, which provides decreased ambient molecules concentration and, as a result, reduced electric field intensification and (4) decreased ion-ion recombination rate (see Fig. 5(IV)).

The first fact takes place because negative streamer corona is full of negatively charged streamer remnants. Despite free electrons quickly turn into the form of negative ions, in equilibrium there is always a fraction of electrons, which obeys the relation:

$$\frac{\nu_{det}}{\nu_{att}} = \frac{n_e}{n_n}. \tag{41}$$

The second case is because, according to relation (8), there are atomic oxygen atoms in the multiple streamer channels, which are generated by negative streamer heads and responsible for the detachment frequency (24). The third and the fourth things are provided with gas heating taking place because of Joule heat release in the streamer channel, which leads to the corresponding gas pressure reduction. So, specific conditions in multiple channels left by negative streamer heads contribute retrograde propagation of positive streamers arising from space stem precursors. Moreover, this effect is even more significant at the close vicinity of the ionization wave, the formation of which demands the joint action of multiple negative streamers.

So, we assume that the space stem precursor is formed as it is capable of emanating a positive streamer, that is, as the condition (38) is met. Note that the same criterion was used by *Cai et al* [2017], who modeled initiation of positive streamer corona in low thundercloud fields occurring via the convergence of a pair of spherical hydrometeors.

Space stem precursor formation times under different both altitudes above sea level h and numbers of negative streamers n_{str} stopping inside the simulation domain each 2.5 ns, which correspond to different values of parameter η, are presented in Table 2 and shown in Fig. 6. It's follows from the Table 2 that under analyzed conditions the model predicted space stem precursor formation time t_{s-f} varies from dozens of nanoseconds up to microseconds. As model data parameterization shows, the space stem precursor formation time can be presented as a function of spatiotemporal frequency of streamer heads appearance inside the simulation domain η (see Fig. 6a):

$$t_{s-f}(\eta)[\mu\text{s}] = \frac{8.81 \cdot 10^{-2}}{\left(\eta/\tilde{\eta} - 2 \cdot 10^{-4}\right)^{0.564}}, \tag{42}$$

where $\tilde{\eta} = 10^{16}$ m^{3}s^{-1}. Space stem precursor formation time as a function of both h and n_{str} can be parameterized as (see Fig. 6b)

$$t_{s-f}(h, n_{str})[\mu\text{s}] = 0.392 \exp\left(0.143h[\text{km}] - 0.14n_{str}\right). \tag{43}$$

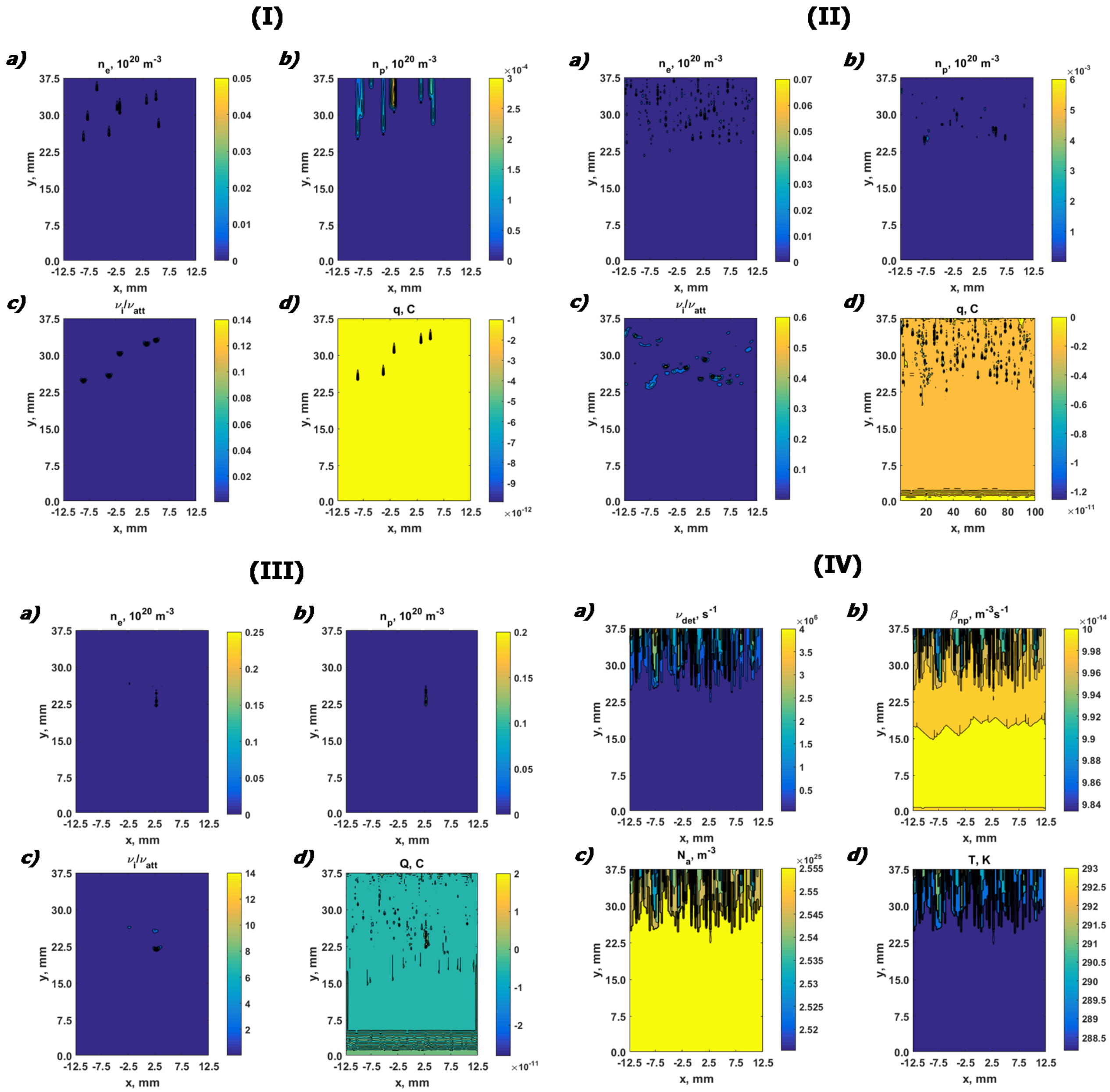

Figure 5. Simulation results obtained for the ground level pressure under η=1.7·10^{15} (n_{str}=5). Subfigures (I)-(III) present (a) electrons and (b) positive ions reduced concentrations, (c) the ratio of ionization frequency to attachment one and (d) the total system charge for (I) initial, (II) middle, and (III) the final space stem precursor development stages (the corresponding moments of time from the start of simulation are 7.5, 52.5, and 109.7 ns, respectively). Subfigure (IV) presents favorable conditions prepared by multiple negative streamers for positive ones, initiating from the space stem precursor: (a) increased detachment frequency and (d) gas temperature and (b) reduced ion-ion recombination rate and (c) neutral molecules number density.

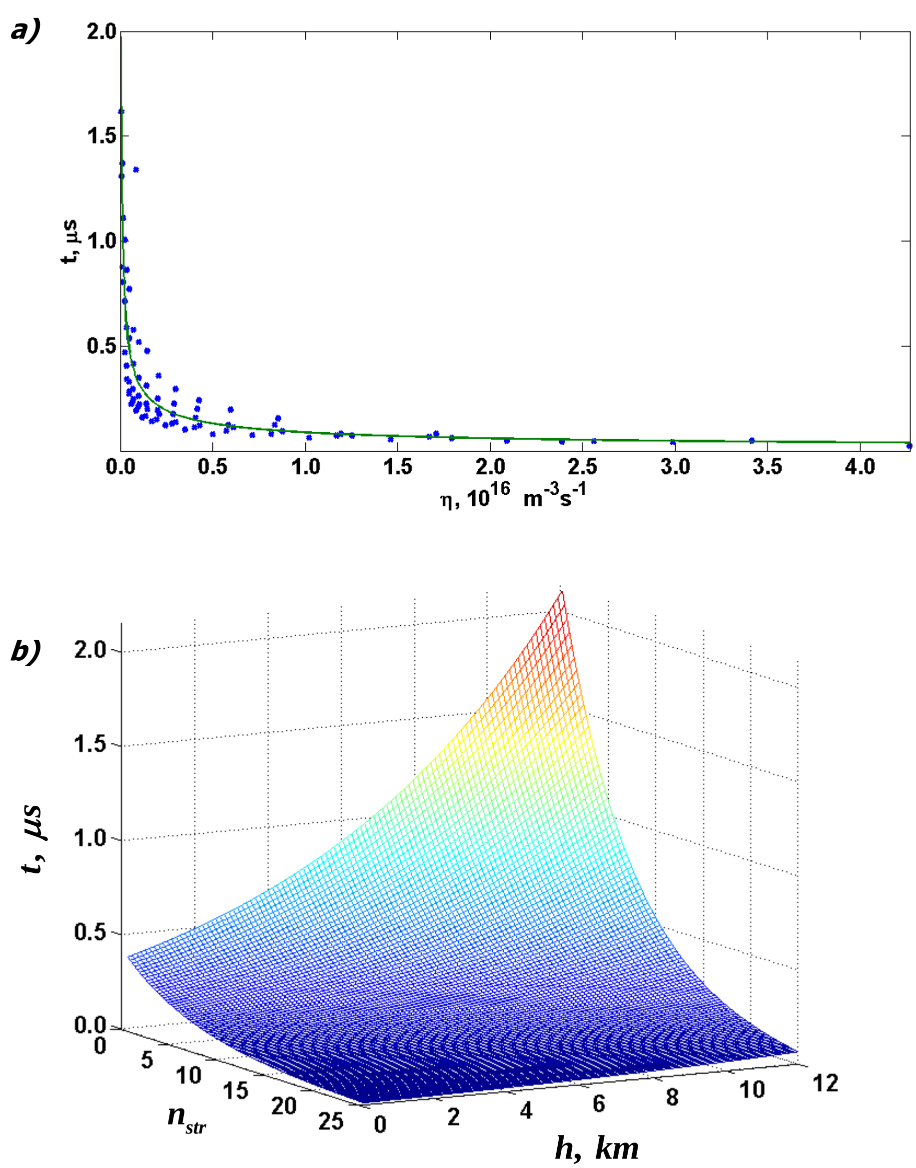

Figure 6. Space stem precursor formation time depending on (a) spatiotemporal frequency of streamer head appearance inside the simulation domain η and (b) both altitude above sea level h and number of streamer heads n_{str} invading the simulation domain per 2.5 ns. Both figures visualize parameterizations (42) and (43) of data given by Table 2.

In this study we restrict ourselves with the fulfillment of Meek's criterion, assuming this as a first step of space stem formation. Description of further space stem evolution, when it (1) collects negative charge via positive streamer system intensification, (2) emanates negative streamers, and (3) gradually transforms into bipolar space leader demands higher spatial resolution needed for the streamer head dynamics modeling than that used in our model (the minimum value of a obtainable under the ground pressure is 2.5·10-4 m) and is beyond the scope of the present study.

Table 2. Space stem precursor formation time $t_{s\text{-}f}$ under different values of altitude above sea level h and number of negative streamers n_{str} stopping at the negative corona streamer burst edge each 2.5 ns.

$t_{s\text{-}f}$, ns		n_{str}					
		25	20	15	10	5	2.5
h, km	0	23.2	49.0	45.5	81.0	154.6	241.2
	1	42.1	44.7	61.2	80.8	196.2	294.7
	2	49.0	67.9	73.4	124.6	200.9	358.5
	3	54.1	72.5	93.0	123.4	225.0	476.4
	4	62.0	80.3	112.3	158.3	250.0	518.3
	5	74.3	94.8	121.5	175.5	311.8	577.1
	6	80.0	112.5	137.5	193.9	347.5	771.6
	7	102.5	130.8	175.0	225.0	415.8	862.5
	8	122.5	150.0	197.5	262.5	537.5	1006.0
	9	140.0	165.0	222.5	295.0	588.0	1110.0
	10	160.0	210.0	247.5	330.0	714.5	1370.0
	11	192.5	235.0	285.0	405.0	805.0	1310.0
	12	222.5	272.5	342.5	470.0	875.0	1617.5

DISCUSSION

It's clear that there must be some specific conditions at the areas of a space stem precursor formation. Since there are no more than a few space leaders simultaneously existing in front of the negative leader tip (see, for example, [*Petersen and Baseley*, 2013; *Hill et al.*, 2011; *Qi et al.*, 2017]), the amount of space stems, arising between two consecutive steps, can't be very large. So, one may consider space stem appearance as an exponentially rare event (a miracle). We suppose that space stems can appear at domains, which are distinguished by increased level of spatiotemporal frequency of streamer heads appearance η. As we consider just a negligibly small fragment of the negative leader corona streamer burst, it would be permissibly to deliberately consider the favorable case of increased values of η inside the simulation domain. In this work, we consider the situation when $\eta=(10^4\text{-}10^5)\eta_a$ (see Fig. 6a). Note that although in our model we for simplicity assume that increased level of η takes place over the entire simulation domain volume, the real areas of increased value of η may have much smaller scale. Actually, this is enough to create favorable conditions at the scale of several streamer radii. The fact of presence of such specific areas may be connected with the peculiarities of small scale potential relief distribution. As the negative streamer corona is a fractal object, electric field inside its volume cannot be constant but vice versa must be strongly heterogeneous. There must be the strongly stochastised local electric field relief, which forces numerous negatively charged streamer heads to get into one and the same area of space despite Coulomb repulsion.

In this study we consider that all streamer heads have the same charge of 10^{-11} C. This is because the well known streamer branching process arising because of Coulomb repulsion. Streamer heads, which contain relatively big amount of charge, are prone to divide into several weaker streamers with less charged heads. So, we suppose that those streamers, which reach the negative corona streamer burst periphery, were produced as a result of multiple branching and, regardless of charge inside initial streamers (emanated from the very negative leader tip), exhausted the capability for division and have the minimal possible charge of 10^{-11} C. This is because the typical scale at which positive streamer branching occurs is of the order of millimeters, while the negative corona streamer burst length at ground level is of the order of several meters and even more for higher altitudes. In this work, we neglect the fact that streamers less branch under decreased pressure and that negative streamers are less incline to branch that positive ones [*Nudnova*, 2009].

In our model we neglect the influence of still moving streamers. All characteristics of a moving streamer are assumed to be stationary (in other words, they are considered as functions of $\left(y - \mathrm{v}_{str} t\right)$) at the coordinate system moving together with the unaltered streamer head. Because of this the electric field of "alive" streamer is strongly localized at the scale of its head, which is about 100 μm for extremely weak streamers we consider in this model. This fact excludes the possibility of any collective effects, which are responsible for the ionization centers formation. After a streamer stops propagation its head is no more capable to remain strongly localized and spreads out over the space because of Coulomb repulsion. As streamer head remnants are distributed over a larger area of space, they can't create such a strong electric field by themselves, but they can overlap in space and time, which results in ionization center formation via directed percolation effect.

To verify simulation results, we must define limits of space stem precursor formation time t_{s-f} variation. It's natural to assume, and calculations confirm this (see Table 2), that the value of t_{s-f} rapidly decreases with increasing η and can be arbitrarily small for sufficiently big values of η. The upper bound of the stem formation time $\overline{t_{s-f}}$, however, can be estimated as (see Fig. 7)

$$\overline{t_{s-f}} = t_{is} - t_b - t_p, \qquad (44)$$

where t_p is time needed for just formed positive space leader to reach the negative leader tip. The relation (44) assumes that at least one space stem must be formed during the interstep time $t_{is} = 10 - 20$ μs to reproduce the negative leader development. If we assume that the positive space leader propagates with the speed of the order of 10^6 m/s [*Gamerota et al.*, 2014], its head must cross the 5-10 m gap between the space stem initiation point and the negative leader tip for t_p=5-10 μs (we neglect slow advancement of the negative leader tip between steps). Assuming that t_b=5-10 μs (see section 2), this means that $\overline{t_{s-f}}$ can't be more than a few microseconds. In this work we set $\overline{t_{s-f}} = 2$ μs as an upper limit of stem formation time for ground level conditions. Since all the characteristic times t_{is}, t_b, and t_p increase with increasing height (decreasing gas pressure), t_{s-f} must also increase with height.

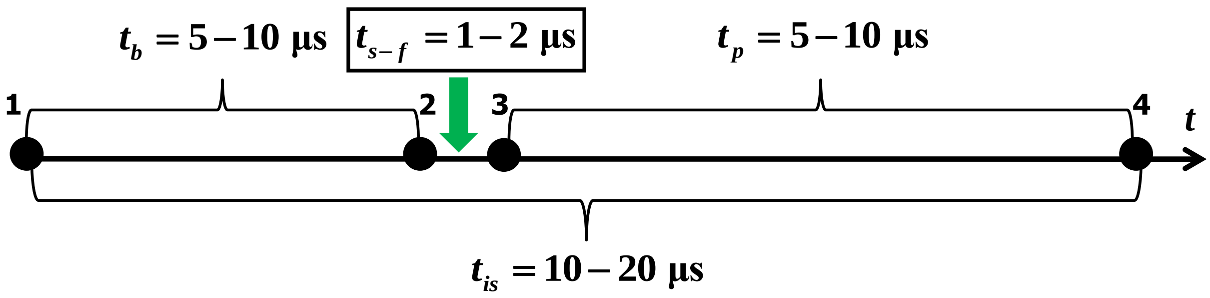

Figure 7. Time diagram of processes involved in lightning negative leader step formation process presented here for ground level pressure (see text). Figures denote the moments of: (1) the start of the negative corona streamer burst finishing the former negative leader step formation and (2) its end, (3) space leader formation, and (4) connection of the positive part of space leader with the negative leader tip leading to its nearly instantaneous jump to the end of the negative part of space leader and the next negative corona streamer burst from the newly-formed negative leader tip (the entire step formation process takes about 1 μs). The presented scheme is designed to show that the space stem formation time is strongly limited and can't be more than several microseconds (the upper limit of space stem precursor formation time in our model is set to 2 μs for ground level pressure).

The increase of space stem precursor formation time t_{s-f} with increasing height can be explained as follows. At first, the scale of negative streamer heads and, respectively, their remnants, according to the similarity law *pd=const*, increase with height. This means that for bigger altitudes streamer head charge is distributed over a bigger area of space and has weaker electric field and, as a result, weaker capability for ionization. This means that the number of streamer head remnants, joint action of which leads to the ionization center formation, must be bigger than for smaller heights. At the second, electron mobility (20.1) also increases with height. This means that domains of locally increased electron number density, that is potential ionization centers, easily spread in space, which prevents the ionization center formation. From the other hand, it follows from Table 2 that sometimes (for relatively small heights) the magnitude of t_{s-f} decreases with increasing height. It may be connected with better mutual overlapping of streamer heads remnants for less pressure, which turns to overcome the effect of their electric field decrement.

It's important that the ambient value of ν_i/ν_{att} is no more than 10^{-2} during the entire simulation time. So, except for several strongly localized areas, the situation is far from the breakdown. But there are small domains, whose space-time volumes are negligible, which are responsible for the specific system behavior. These fractal multiplicities with nearly zero measures have a non-zero probability to turn into space stems. In general, the situation is ideologically close to that which is described in the study of *Iudin* [2017] devoted to the lightning leader initiation via noise-induced kinetic transition.

Although in this study we considered the case of negative lightning leader only, the described mechanism can work for laboratory negative leader too. Since laboratory leader negative corona streamer burst has smaller both scale and total charge thrown off from the newly formed negative leader tip, the values of spatiotemporal noise intensity can be of the same order as for lightning leader case. So, space stem precursor formation time must conserve too.

CONCLUSION

In this study, we propose a new mechanism of space stem precursor formation, which is based on the joint action of impact ionization and drift occurring at the external boundary of the negative corona streamer burst, where electric field strength is amplified. The process takes place in the presence of strongly inhomogeneous stochastic electric field relief, which is formed by chaotically positioned clusters of negative charge transported to the negative corona streamer burst periphery by the negative streamer heads. The only thing needed for the space stem precursor formation is the increased level of streamer heads appearance frequency inside the very small area of space, which scale is of the order of several streamer radii. We analyzed allowable space stem precursor formation times at the range of altitudes of 0-12 km and found that it exponentially decreases with pressure (increases with increasing height). One important conclusion derived from this study is that the relatively strong electric field strength, overabundance of negative charge, and increased level of both reduced electric field and detachment frequency, which accompany ionization center formation, facilitate survival and growth of positive streamers initiated from a space stem precursor.

APPENDIX A: CALCULATION METHOD

As in our model we solve the system of difference equations (38) by the Euler's direct method, it’s important to monitor the calculation correctness. The computational algorithm we use to ensure both non-negative concentration values and charge conservation law is described below.

Let’s consider the system of difference matrix equations (38.1)-(38.3) reduced to the following form

$$\begin{cases} \widetilde{n_e}\,|_{t+1} = \widetilde{n_e}\,|_t + \mathrm{S}_e^+ - \mathrm{S}_e^- \\ \widetilde{n_p}\,|_{t+1} = \widetilde{n_p}\,|_t + \mathrm{S}_p^+ - \mathrm{S}_p^- \\ \widetilde{n_n}\,|_{t+1} = \widetilde{n_n}\,|_t + \mathrm{S}_n^+ - \mathrm{S}_n^- \end{cases}, \tag{A1}$$

where S_e^+, S_p^+, S_n^+ and S_e^-, S_p^-, S_n^- can be defined as sources and sinks in equations for electrons and positive and negative ions, respectively, and are specified as

$$\begin{cases} \mathrm{S}_e^+ = \tau\left(\nu_i \widetilde{n_e}\,|_t + \nu_{det}\widetilde{n_n}\,|_t + \Omega/n_0 + f\left(\vec{r},t\right)\big/n_0 + J_e^+\right) \\ \mathrm{S}_p^+ = \tau\left(\nu_i \widetilde{n_e}\,|_t + \Omega/n_0 + J_p^+\right) \\ \mathrm{S}_n^+ = \tau\left(\nu_{att}\widetilde{n_e}\,|_t + J_n^+\right) \end{cases}, \tag{A2}$$

$$\begin{cases} \mathrm{S}_e^- = \tau\left[\left(\nu_{att} + \beta_{ep} n_0 \widetilde{n_p}\,|_t\right)\widetilde{n_e}\,|_t + J_e^-\right] \\ \mathrm{S}_p^- = \tau\left[\left(\beta_{ep} n_0 \widetilde{n_e}\,|_t + \beta_{np} n_0 \widetilde{n_n}\,|_t\right)\widetilde{\mathrm{n}_p}\,|_t + J_p^-\right] \\ \mathrm{S}_n^- = \tau\left[\left(\nu_{det} + \beta_{np} n_0 \widetilde{n_p}\,|_t\right)\widetilde{n_n}\,|_t + J_n^-\right] \end{cases} . \tag{A3}$$

As for fluxes matrixes J_e^+, J_e^+, J_e^+, and J_e^-, J_e^-, J_e^-, they can be defined as

$$\begin{cases} J_e^+ = \max\left(-div\overrightarrow{J_e}, 0\right) \\ J_e^- = \min\left(-div\overrightarrow{J_e}, 0\right) \\ J_p^+ = \max\left(-div\overrightarrow{J_p}, 0\right) \\ J_p^- = \min\left(-div\overrightarrow{J_p}, 0\right) \\ J_n^+ = \max\left(-div\overrightarrow{J_n}, 0\right) \\ J_n^- = \min\left(-div\overrightarrow{J_n}, 0\right) \end{cases} . \tag{A4}$$

At each model time step we calculate the following lowering coefficients

$$\begin{cases} k_e = \min\left(\mathrm{S}_e^- \big/ \left(\widetilde{n_e}\,|_t + \mathrm{S}_e^+\right), 1\right) \\ k_p = \min\left(\mathrm{S}_p^- \big/ \left(\widetilde{n_p}\,|_t + \mathrm{S}_p^+\right), 1\right) \\ k_n = \min\left(\mathrm{S}_n^- \big/ \left(\widetilde{n_n}\,|_t + \mathrm{S}_n^+\right), 1\right) \end{cases} \tag{A5}$$

and define auxiliary matrixes

$$\begin{cases} Att = k_e \nu_{att} \widetilde{n_e}\,|_t \\ Det = k_n \nu_{det} \widetilde{n_n}\,|_t \\ B_{ep} = \min\left(k_e, k_p\right) \beta_{ep} n_0 \widetilde{n_e}\,|_t\, \widetilde{\mathrm{n}_p}\,|_t \\ B_{np} = \min\left(k_n, k_p\right) \beta_{np} n_0 \widetilde{n_n}\,|_t\, \widetilde{\mathrm{n}_p}\,|_t . \end{cases} \tag{A6}$$

Now the initial system (A1) can be rewritten as

$$\begin{cases} \widetilde{n_e}\,|_{t+1} = \widetilde{n_e}\,|_t + \tau\left(\nu_i \widetilde{n_e}\,|_t + Det + \Omega/n_0 + f\left(\vec{r},t\right)/n_0 + J_e - Att - B_{ep}\right) \\ \widetilde{n_p}\,|_{t+1} = \widetilde{n_p}\,|_t + \tau\left(\nu_i \widetilde{n_e}\,|_t + \Omega/n_0 + J_p - B_{ep} - B_{np}\right) \\ \widetilde{n_n}\,|_{t+1} = \widetilde{n_n}\,|_t + \tau\left(\nu_{att} \widetilde{n_e}\,|_t + J_n - Det - B_{np}\right) \end{cases}. \qquad (A7)$$

Specification of matrixes J_e, J_p and J_n requires special attention. We now consider the case of J_e only, but all discussions given below can be applied to J_p and J_n in the same way. In difference approach the divergence operator calculated in a spatial grid node with indexes $i = 1 : N_x$ and $j = 1 : N_y$ is defined as

$$div\overrightarrow{J_e}\left(i,j\right) = \frac{J_{ex}\left(i,j+1\right) - J_{ex}\left(i,j-1\right) + J_{ey}\left(i,j+1\right) - J_{ey}\left(i,j-1\right)}{2}, \qquad (A8)$$

where components of vector $\overrightarrow{J_e} = \left\{J_{ex}, J_{ey}\right\}$ are

$$\begin{cases} J_{ex} = \mu_e n_e E_x + D_e \dfrac{\partial n_e}{\partial x} \\ J_{ex} = \mu_e n_e E_y + D_e \dfrac{\partial n_e}{\partial y} \end{cases}. \qquad (A9)$$

Note that in our model we consider the simulation plane as a surface of the two-dimensional torus, that is $i = 1$ follows after $i = N_x$ and $j = 1$ follows after $j = N_y$. This is needed to prevent the particles drifting out of the simulation domain. At each model time step and for each spatial grid node we consistently conclude the following operations directed to fluxes recalculation

$$\begin{aligned} &\begin{cases} J_e\left(i,j\right) = J_e\left(i,j\right) + \left(k_e - 1\right) J_{ex}\left(i,j+1\right)/2 \\ J_e\left(i,j+2\right) = J_e\left(i,j+2\right) + \left(1 - k_e\right) J_{ex}\left(i,j+1\right)/2 \\ J_{ex}\left(i,j+1\right) = k_e J_{ex}\left(i,j+1\right) \end{cases} \\ &\begin{cases} J_e\left(i,j\right) = J_e\left(i,j\right) + \left(1 - k_e\right) J_{ex}\left(i,j-1\right)/2 \\ J_e\left(i,j-2\right) = J_e\left(i,j-2\right) + \left(k_e - 1\right) J_{ex}\left(i,j-1\right)/2 \\ J_{ex}\left(i,j-1\right) = k_e J_{ex}\left(i,j-1\right) \end{cases} \\ &\begin{cases} J_e\left(i,j\right) = J_e\left(i,j\right) + \left(k_e - 1\right) J_{ey}\left(i+1,j\right)/2 \\ J_e\left(i+2,j\right) = J_e\left(i+2,j\right) + \left(1 - k_e\right) J_{ey}\left(i+1,j\right)/2 \\ J_{ey}\left(i+1,j\right) = k_e J_{ey}\left(i+1,j\right) \end{cases} \\ &\begin{cases} J_e\left(i,j\right) = J_e\left(i,j\right) + \left(1 - k_e\right) J_{ey}\left(i-1,j\right)/2 \\ J_e\left(i-2,j\right) = J_e\left(i-2,j\right) + \left(k_e - 1\right) J_{ey}\left(i-1,j\right)/2 \\ J_{ey}\left(i-1,j\right) = k_e J_{ey}\left(i-1,j\right) \end{cases}. \end{aligned} \qquad (A10)$$

The same algorithm applies to J_p and J_n with replacement of k_e for k_p and k_n, respectively.

The described algorithm (A2)-(A10) are directed to sinks S_e^-, S_p^-, and S_n^- reduction to the level of sources S_e^+, S_p^+, and S_n^+ at the spatial grid nodes, at which they initially exceeded the corresponding sources. Otherwise, calculations can lead to both negative concentration values and charge conservation law violation. It's important that the described sinks reduction procedure saves relative contributions of each term in relation (A3). Note that the set of operations (A10) leads to fluxes variation not only at the node with the coordinate numbers (i, j), but also at the nearest nodes, characterizing by $(i \pm 1, j)$, $(i, j \pm 1)$, $(i \pm 2, j)$, and $(i, j \pm 2)$ coordinate numbers. Because of this described fluxes recalculation leads to variations in sources (A2) and sinks (A3) matrixes, which can affect the lowering coefficient matrixes (A5). To minimize the calculation error caused by described sequence of operations, we at repeat algorithm (A2)-(A10) 100 times at each model time iteration. Calculation shows that applied method converges (calculation error at least doesn't increase at any cycle step), which ensures the high degree of calculation accuracy: the deviation from the charge conservation law doesn't exceed 1%.

REFERENCES

1. Babich, L. P., E. I. Bochkov, I. M. Kutsyk, T. Neubert, and O. Chanrion (2016), Positive streamer initiation from raindrops in thundercloud fields, *J. Geophys. Res.*, 121, 11, 6393–6403, doi:10.1002/2016JD024901.
2. Bazelyan, E. M., B. N. Gorin, and V. I. Levitov (1975), Some problems of research of the leader breakdown in air, *Izv. Akad. Nauk SSSR, Energetika i Transport* (in Russian), 5, 30–38.
3. Bazelyan, E. M., and Y. P. Raizer (2000), *Lightning Physics and Lightning Protection*, Institute of Physics Publishing, Bristol, Philadelphia.
4. Benilov, M. S. and G. V. Naidis (2003), Modelling of low-current discharges in atmospheric-pressure air taking account of non-equilibrium effects, *J. Phys. D: Appl. Phys.*, 36, 1834–1841.
5. Cai, Q., Jánský, J., and Pasko, V. P. (2017), Initiation of positive streamer corona in low thundercloud fields, *Geophys. Res. Lett.*, *44*(11), 5758-5765, doi:10.1002/2017GL073107.
6. Dubinova, A., C. Rutjes, U. Ebert, S. Buitink, O. Scholten, and G. Thi Ngoc Trinh (2015), Prediction of lightning inception by large ice particles and extensive air showers, Phys. Rev. Lett., 115, 015002, doi:10.1103/PhysRevLett.115.015002.
7. Dutton, J. (1975), A survey of electron swarm data, J. Phys. Chem. Ref. Data, Vol. 4, No 3, p. 730.
8. Gamerota, W. R., V. P. Idone, M. A. Uman, T. Ngin, J. T. Pilkey, and D. M. Jordan (2014), Dart-stepped-leader step formation in triggered lightning, Geophys. Res. Lett., 41, 2204–2211, doi:10.1002/2014GL059627.
9. Gorin, B. N. and A. V. Shkilev (1976), The development of electrical discharge in long gaps rod-plane with a negative voltage pulse, *Elektrichestvo* (in Russian), 6, 31–39.

10. Gurevich, A. V., G.M. Milikh, and R. Roussel-Dupre (1992), Runaway electron mechanism of air breakdown and preconditioning during a thunderstorm, *Phys. Lett. A.*, Vol. 165, 463-468.
11. Gurevich, A. V., and K. P. Zybin (2001), Runaway breakdown and electric discharges in thunderstorms, *Phys.-Uspekhi*, Vol. 44(11), 1119-1140.
12. Hill J. D., M.A. Uman, and D.M. Jordan (2011), High-speed video observations of a lightning stepped leader, J. Geophys. Res., 116, D16117, doi:10.1029/2011JD015818.
13. Iudin, D. I. (2017), Lightning-Discharge Initiation as a Noise-Induced Kinetic Transition, *Radiophys Quantum El*, Vol. 60, No. 5, 374-394, doi.org/10.1007/s11141-017-9807-x.
14. Ivanovskiy, A.V. (1996), On streamer breakdown of air in a homogeneous electric field, *Tech. Phys.* (in Russian), 66(8), 59-72.
15. Kostinskiy, A. Yu., V. S. Syssoev, N. A. Bogatov, E. A.Mareev, M. G. Andreev, M. U. Bulatov, D. I. Sukharevsky, and V. A. Rakov (2017), Abrupt Elongation (Stepping) of Negative and Positive Leaders Culminating in an Intense Corona Streamer Burst: Observations in Long Sparks and Implications for Lightning, *J. Geophys. Res. Atmos*., in review.
16. Les Renardieres group (1981), Negative discharges in long air gaps at Les Renardieres - 1978 results, *Electra*, 74, 67–216.
17. Loeb, L. B (1966), The mechanism of stepped and dart leaders in cloud-to ground lightning strokes, *J. Geophys. Res.*,Vol. 71(20), 4711-4721.
18. Minyaev, V. V. (2004), Computation of Atmosphere Parameters Considering Air Humidity, *Bulletin of MSTU. N.E. Bauman. Ser. "Natural Sciences"* (in Russian), № 2, 106-120.
19. Nudnova, M. M. (2009), *Dynamics and structure of ionization waves in the nanosecond range under high overvoltages at various discharge gap configurations*, PhD thesis, Moscow, 121 pp.
20. Petersen, D., M. Bailey, W. H. Beasley, J. Hallett (2008), A brief review of the problem of lightning initiation and a hypothesis of initial lightning leader formation, *J. Geophys. Res.*, 113, D17205, doi:10.1029/2007JD009036.
21. Petersen, D. A., and W.H. Beasley (2013), High-speed video observations of a natural negative stepped leader and subsequent dart-stepped leader, *J. Geophys. Res. Atmos.*, 118, 12,110-12,119, doi:10.1002/2013JD019910.
22. Qi Q., W. Lua, and Y. Ma, L. Chen, Y. Zhang, and V. A. Rakov (2016), High-speed video observations of the fine structure of a natural negative stepped leader at close distance, *Atmos. Res.*, 178-179, 260-267, doi: 10.1016/j.atmosres.2016.03.027.
23. Raizer, Y. P. (1991), *Gas Discharge Physics*, Springer, New York.
24. Raizer, Y. P. (2009), *Gas Discharge Physics* (in Russian), Intellect, Dolgoprudny.
25. Rakov, V. A., and M. A. Uman (2003), *Lightning: Physics and Effects*, Cambridge Univ. Press, New York.
26. Sadighi, S., N. Liu, J.R. Dwyer, and H. K. Rassoul (2015), Streamer formation and branching from model hydrometeors in subbreakdown conditions inside thunderclouds, *J. Geophys. Res. Atmos.*, 120, 3660-3678, doi:10.1002/2014JD022724.

27. Uman, M.A. (1969), *Lightning*, McGraw Hill, New York.